# REDUCED SHAFT STIFFNESS LOWERS RUNNING-SPEED BEARING LOADS AND VIBRATION IN A SINGLE STAGE COMPRESSOR

by

**Richard W. Armentrout**

**Rotating Machinery Consultant**

**Pacific Gas and Electric Company**

**San Ramon, California**

**and**

**Gerald E. Wilson**

**Mechanical Maintenance Engineer**

**Chino Mines Company, Phelps Dodge Corporation**

**Hurley, New Mexico**

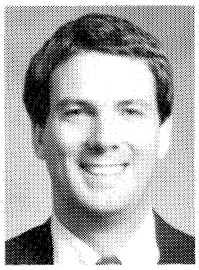

*Richard W. Armentrout is a Rotating Machinery Consultant with Pacific Gas and Electric Company in San Ramon, California, where he conducts rotordynamic design audits, hydrodynamic bearing design analyses, and structural vibration studies in support of the various power generation facilities within PG&E. Prior to joining PG&E, Mr. Armentrout worked for various bearing companies including KMC Division of Cookson America, and Centri Marc Division of Imo Industries, where he designed fluid film bearings and conducted rotordynamics studies of a wide variety of turbomachinery. Mr. Armentrout has also worked in structural dynamics at McDonnell Douglas, Martin Marietta, and Westinghouse. While at McDonnell Douglas, he designed a passive vibration isolation system for a zero-gravity exercise treadmill to be used on Space Station Freedom.*

*Mr. Armentrout received his B.S.M.E. (1978), and M.S.M.E. (1983) degrees from the University of Virginia. While at the University of Virginia, he conducted experimental research in the areas of hydrodynamic bearings and FFT modal testing of rotor-foundation structures.*

*Gerald Wilson is Maintenance Manager for Chino Mines Company, division of Phelps Dodge Corporation, located at Hurley, New Mexico, where he is responsible for vibration analysis, alignments, troubleshooting, system design, and system revisions.*

*Prior to Chino Mines Company, he worked with NASA as a Rocket Test Engineer at the Las Cruces, New Mexico, facility where he was Test Conductor on various testing of NASA components and systems. He also was involved with cryogenic testing of materials.*

*Mr. Wilson attended New Mexico Military Institute, Northrup Institute of Technology, and New Mexico State University in the Mechanical and Chemical Engineering fields.*

## ABSTRACT

Turbomachines that run well above their fundamental lateral critical speeds (super-resonant), and are not heavily influenced by higher vibrational modes, can often benefit from reductions in shaft stiffness to lower the running-speed bearing loads and vibration. This is because an unbalanced rotor running in the super-resonant regime tends to orbit eccentrically about its offset center of gravity, causing high bearing loads if the shaft is rigid. A more flexible shaft can deflect and reduce the dynamic force transmitted into the bearings, resulting in better bearing life and lower system vibration. In many cases, this can be done without lowering the damping enough to adversely affect the rotordynamic stability and unbalance response characteristics of the machine. A case study is presented in which a single-stage overhung compressor was modified to a smaller shaft diameter, yielding a beneficial 48 percent reduction in the computed bearing dynamic loads at running speed that improved bearing life and lowered the operating vibration levels.

## INTRODUCTION

Traditional design practice in many types of turbomachinery, especially in overhung machines, has been to make the shaft large in diameter (rigid) to maximize the bearing motion for good system damping. A rigid shaft maximizes damping by concentrating the modal displacement in the bearing oil film where the damping is high, rather than in shaft deflection where the damping is low. This is beneficial when the rotor traverses the first critical speed, where attenuation of the resonant response depends on modal damping from the oil film to limit the rotor motion. However, in machines that pass through their first critical speed to higher operating speeds, the rotor motion is no longer resonant, but rather is self-limiting at a value approximately equal to the rotor mass unbalance eccentricity. In this regime, a stiff shaft is detrimental, because it transfers the rotor orbital motion into the bearings, causing high bearing loads and casing vibration. Such rigid-shaft machines reflect a common tendency among rotor designers to favor rigid shafts to maximize damping, improve stability, and assure adequate strength to carry the lateral and torsional forces necessary for power transmission in the machine. Often, however, these design objectives are overemphasized, resulting in shafts that are far more rigid than required to yield satisfactory machine performance. Consequently, there are many machines in operation with higher than necessary shaft stiffnesses,

causing unnecessarily high bearing loads and vibration at running speed. As with any major design change, reasonable caution must be exercised, as some types of machines depend on a minimum shaft stiffness to maintain rotordynamic stability.

A case study is discussed of the single stage compressor shown in Figure 1, in which a reduction of shaft diameter (stiffness) between the bearings yielded a beneficial 48 percent reduction in the computed dynamic bearing loads at running speed. This load reduction, in combination with the installation of high load capacity spherical pivot tilting pad bearings, extended the original three month service intervals to well above one year.

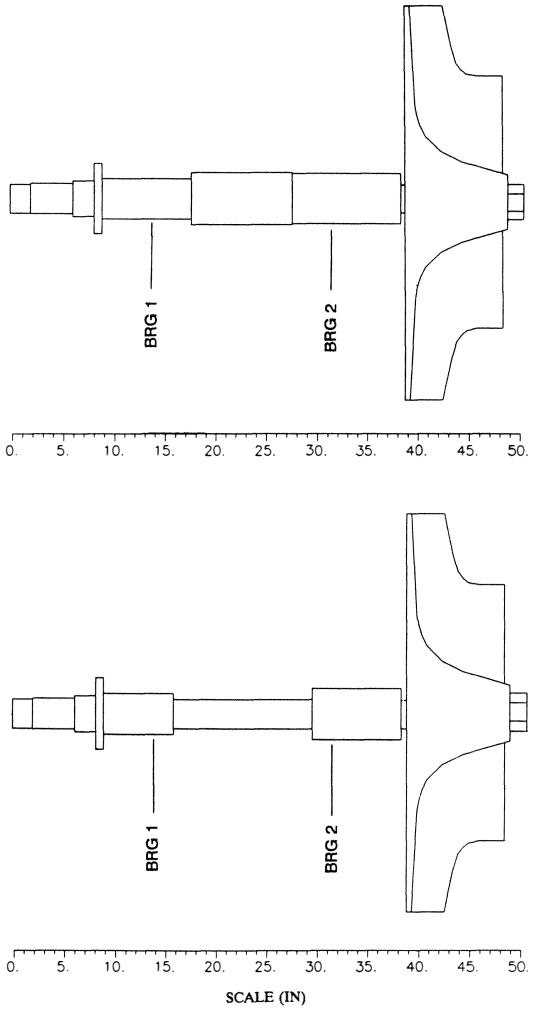


*Figure 1. Original and Modified Compressor Rotors.*

As illustrated in Figure 1, the compressor has bearings that are relatively closely spaced, with a large overhung impeller mounted outboard of the bearings. The original stiff shaft of the compressor overloaded the bearings at running speed after the impeller became unbalanced from erosive and corrosive working gasses, resulting in high bearing dynamic loads and excessive bearing wear.

The revised rotor geometry incorporates a more flexible rotor as shown in the bottom of Figure 1, where the shaft diameter has been reduced from 5.0 in to 2.8 in between the bearings. The bearings were also upgraded from the original rocker pivot tilting pad bearings to a set of high load capacity spherical pivot tilting pad bearings. Optimization of the new shaft-bearing system was found to dramatically reduce the running speed bearing loads, while maintaining sufficient modal damping at the first critical speed to adequately attenuate the first mode as it is traversed during startup and coastdown.

A number of authors [1, 2, 3, 4] have studied the effects of rotor and support stiffness on the unbalance response and bearing loads in turbomachinery. Gunter [4] demonstrated the benefits of rotor and support compliance in reducing bearing loads in a machine similar to the one discussed here. Some of the performance advantages of the reduced running-speed bearing loads include:

- Tilting pad bearing pivot stresses are reduced, promoting longer bearing life and enhanced reliability.
- Transmitted pedestal and foundation forces are reduced, thus lowering overall system vibration for quieter, more reliable operation at running speed.
- Higher rotor unbalance is tolerable for a given trip level of vibration, thus extending shutdown intervals for rotor rebalancing.

For assurance of continued shaft integrity, a complete reanalysis of the steady state and transient bending stresses, torsional stresses, and torsional natural frequencies was conducted to assure that the smaller shaft was not overstressed or in danger of an adverse torsional resonance. The rotordynamic analysis and principles incorporated in the design upgrades are presented in the sections that follow.

## PRINCIPLES OF ROTOR UNBALANCE RESPONSE

The effects of rotor unbalance vary dramatically in the subresonant, resonant, and super resonant operating regimes. It is useful to examine the response characteristics in each of these ranges to understand the response behavior exhibited by the overhung compressor. This may be done through the use of simple single-mass models whose equations of motion are easily derived (APPENDIX). The principles exhibited by the simple models may then be extended to the actual compressor rotor for a basic understanding of its response characteristics.

### *Overhung Rotor Characteristics*

The Jeffcott rotor equations of motion (presented in the APPENDIX) yield three different limiting values for the rotor disk vibration depending on whether the speed is well below (subresonant), equal to (resonant), or well above (super resonant) the first critical speed. The three limiting disk response amplitudes, $X_o$, are:

$$\begin{aligned} X_o &\simeq 0 \quad \text{(subresonant)} \\ &= \frac{u_b}{2\xi} \quad \text{(resonant)} \\ &\simeq u_b \quad \text{(super resonant)} \end{aligned} \tag{1}$$

where:

$u_b$ = Unbalance eccentricity (in)

$\xi$ = Dimensionless damping ratio

$= C/C_c$

$= C/2(KM)^{1/2}$

These response limits may be illustrated for an overhung rotor using the single-mass model shown in Figure 2. Neglecting the second order gyroscopic and rotary inertia effects, the same single degree of freedom expression derived for the Jeffcott rotor may be applied to the overhung rotor. Like the Jeffcott rotor, this means that the eccentricity at speeds well above the first critical speed will approach the static disk unbalance eccentricity, $U_b$.

The animated first mode shape of the overhung model is shown in Figure 3. The computed speed-dependent unbalance response

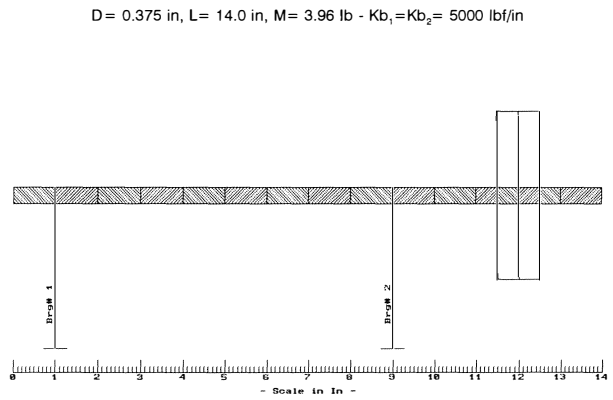


*Figure 2. Single-Mass Overhung Rotor Model.*

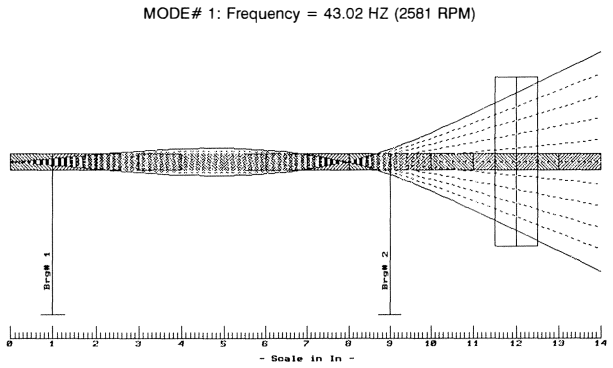


*Figure 3. Single-Mass Overhung Rotor First Mode Shape.*

for 0.035 oz-in of unbalance at the disk is plotted in Figure 4. Applied to the 3.55 lbm disk, the unbalance of 0.035 oz-in yields a disk unbalance eccentricity of

$$U_b = \frac{0.035 \text{ oz-in}}{(3.55 \text{ lbm})(16\text{oz/lbm})} = 0.00061 \text{ in} \qquad (2)$$

Bearing coefficients corresponding to a simple 3/8 in diameter two-axial-groove oil lubricated bearing were used.

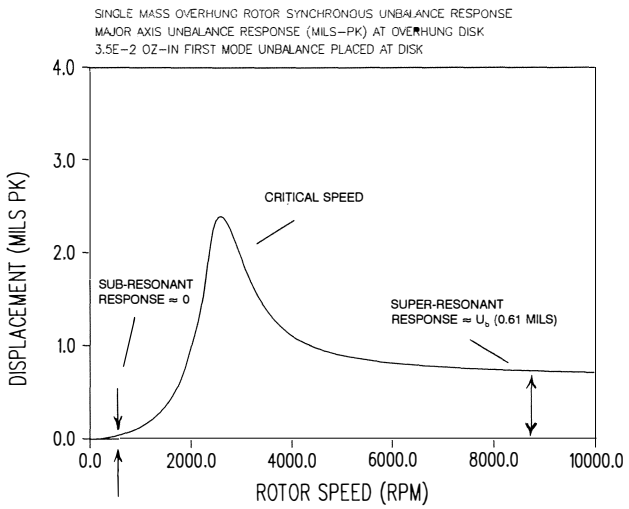


*Figure 4. Single-Mass Overhung Rotor Unbalance Response.*

As expected, the response behavior is very similar to that predicted by Equation (1). At very low, subresonant speeds, the disk geometric center is almost coincident with the bearing centerline, yielding nearly zero unbalance response. Above the critical speed, the offset disk CG seeks the bearing centerline, resulting in nearly constant unbalance response that approaches the disk unbalance eccentricity of 0.61 mils.

*Cantilever Beam Model*

Through the above discussion, it has been shown that at speeds well above the first critical speed, an overhung disk will tend to orbit eccentrically about its mass center, regardless of the shaft stiffness, bearing stiffness, or bearing damping. This means that the rotor-bearing system may be analyzed as a static cantilever beam on flexible supports (to represent the bearings) with a known end displacement representing the disk (impeller) orbit eccentricity, $U_b$.

A simply supported cantilever beam model of the compressor shaft on flexible supports is illustrated in Figure 5. The bearing stiffnesses, $K_1$ and $K_2$, act in series with the shaft stiffness to support the overhung impeller. Using the equations for a cantilever beam on flexible supports, the bearing reaction forces may be written in terms of the impeller displacement, $\delta_{imp}$, as:

$$R_1 = \frac{-\delta_{imp}}{\frac{abL}{3EI} + \frac{b}{K_1 a} + \frac{L^2}{K_2 ab}}$$

$$R_2 = \frac{\delta_{imp}}{\frac{b^2 a}{3EI} + \frac{b^2}{K_1 aL} + \frac{L}{K_2 a}} \qquad (3)$$

where:

$R_1, R_2$ = Bearing reactions (lbf)
$\delta_{imp}$ = Impeller end displacement (in)
a,b,L = Rotor and support dimensions (in)
$K_1, K_2$ = Bearing stiffnesses (lbf/in)
I = Shaft area moment of inertia ($in^4$)
E = Shaft material modulus of elasticity ($lbf/in^2$)

It is evident from these equations that a reduction in the shaft stiffness through a decrease in its cross sectional moment of inertia, I, will decrease the bearing loads, $R_1$ and $R_2$. Consequently, the potential effectiveness of reduced shaft stiffness in unloading the bearings is revealed directly by the cantilever beam equations.

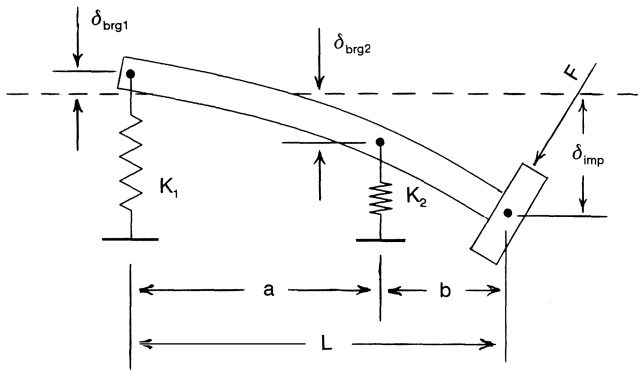


*Figure 5. Elastically-Supported Cantilever Beam.*

These effects may be illustrated schematically using two elastically supported shafts of different stiffness under the same end displacement as shown in Figure 6. When the shaft is stiff, the rigidity transfers the impeller eccentricity directly into the bearings, resulting in high bearing motion and loads. Reduction of the shaft diameter allows the shaft to deform and absorb much of the impeller eccentricity before it reaches the bearings, yielding a significant reduction in bearing loading for the same impeller eccentricity. Since unbalance response is synchronous, the shaft deflection is static in the rotating reference frame, and thus does not subject the shaft to fatigue from reverse bending.

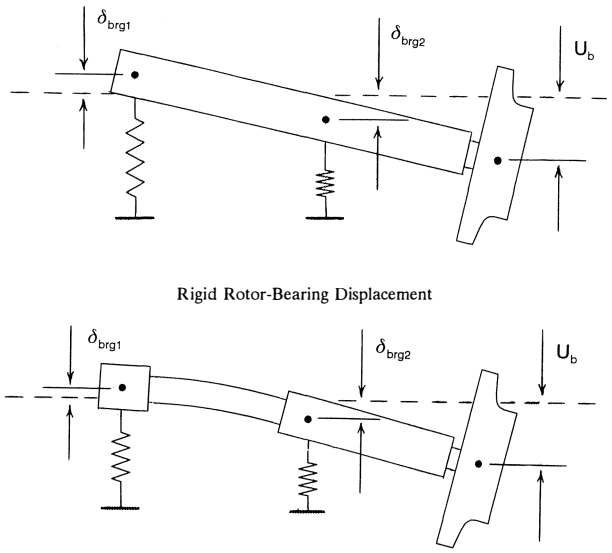


*Figure 6. Rigid and Flexible Rotor-Bearing Displacement Due to Impeller Eccentricity.*

## CASE STUDY—SINGLE STAGE COMPRESSOR

### *Background and History*

An overhung centrifugal plant air handling compressor running 24 hr/day in the field was experiencing frequent machine outages due to excessive bearing wear at running speed. As the impeller became unbalanced from gas erosion, the running-speed bearing dynamic loads would fatigue the pad pivots on the rocker-pivot tilting pad bearings, causing excessive bearing clearances that would raise the vibration levels and trip the machine off line. Frequent (approximately every three months) bearing overhauls were required to keep the machine operational.

Because of the persistent reliability problems with the air compressor, the customer was interested in upgrading the machine beyond the conventional "patch up" type of repair. Rather, he was seeking a comprehensive reanalysis and fundamental redesign that would permanently correct the running speed vibration problems exhibited by the compressor. This required an in depth study of the principles affecting the rotordynamic performance of the compressor.

The following sections summarize the rotordynamic analyses and design optimization conducted to fulfill the customer's requirements. Unbalance response data is presented to illustrate the effectiveness of the reduced shaft stiffness in modifying the rotordynamic behavior at running speed. The original shaft rotordynamics are presented for comparison to the revised rotor characteristics. Bearing dynamic loads *vs* speed are plotted for both the original and revised shaft geometries, showing the dramatic reduction in bearing loads afforded by the lower shaft stiffness.

### *Compressor Description*

The compressor studied is a single stage, axial-to-radial flow, centrifugal blower typical of many machines in service throughout the petrochemical, manufacturing, and power generation industries. Overall compressor specifications are as follows:

| | |
|---|---|
| Rotor Type: | Single-Stage Overhung Motor Driven Centrifugal Compressor |
| Nominal Running Speed: | 6,300 rpm |
| Impeller Diameter: | 39.5 in |
| Rotor Weight: | 625.0 lb |
| Rotor Length: | 50.2 in |
| Bearing Span: | 17.5 in |
| Maximum Power: | 3,500 hp |

### *Undamped Critical Speeds*

Illustrated in Figure 7 are the rotor computer models for the original and revised shafts with the respective computed undamped critical speed mode shapes superimposed. In both plots, the bearing stiffnesses were varied with speed, so that they would represent the approximate speed-dependent bearing dynamic stiffnesses. The pedestal mass and stiffness were estimated at 500 lbm and $2.0 \times 10^6$ lbf/in, which represent typical values for machines of this type and size. The undamped critical speed map for the original and revised shafts is plotted in Figure 8. The bearing dynamic stiffness curve is also plotted on the map. Here, the bearing stiffness curve represents the average between the impeller end and thrust end horizontal and vertical dynamic stiffness for the replacement tilting pad bearings on flexible pedestals. Therefore, the intersections of the bearing curve with the critical speed curves represent the predicted damped critical speeds.

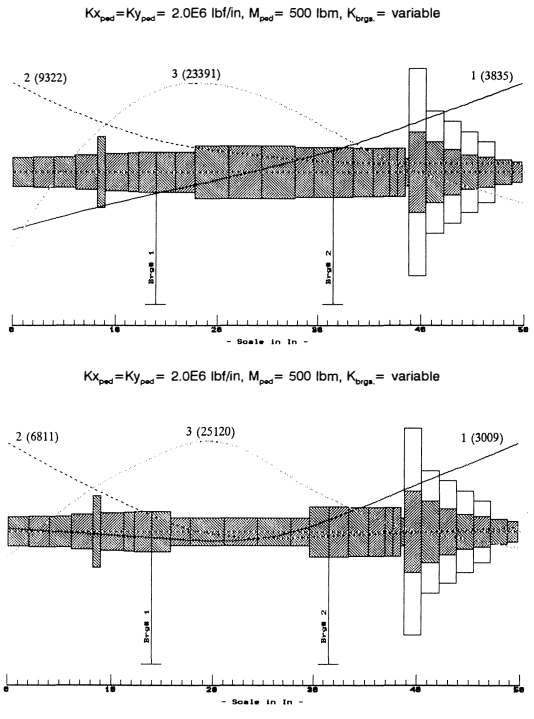


*Figure 7. Compressor Computer Models and Undamped Mode Shapes.*

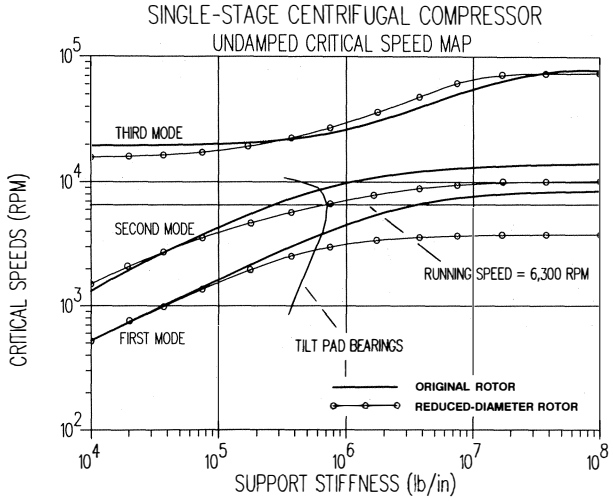


*Figure 8. Compressor Undamped Critical Speed Map.*

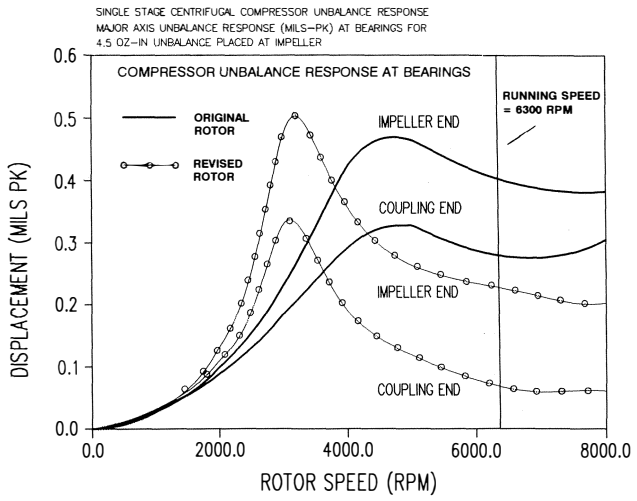


*Figure 9. Computed Compressor Unbalance Response at Bearings.*

The first critical speed is the classic rigid rotor conical mode typical of overhung machines with short bearing spans. Because nearly all of the modal compliance is in the bearings, rather than the shaft, the bearing damping is very effective, making this a well attenuated mode that is relatively insensitive to unbalance. Since nearly all of the modal strain energy is in the bearings, this mode is very sensitive in both frequency and magnitude to bearing stiffness and damping changes. The first mode frequency is 3835 rpm with the original stiff shaft, and is lowered to 3009 rpm with the more flexible rotor. Comparison of the mode shapes indicates that the more flexible rotor exhibits greater midspan bending than the stiff rotor, which is the beneficial additional compliance that will be shown to absorb some of the impeller eccentricity to unload the bearings at running speed.

The second critical speed is a cantilever mode of the thrust end of the rotor. Unlike the first mode, there is now much more shaft bending relative to bearing displacement in the mode shape, making this a less attenuated mode that is more sensitive to unbalance. The second mode frequency is lowered from 9322 rpm with the original shaft to 6811 rpm with the revised shaft geometry. Although this places the second mode very near the running speed of 6300 rpm, it is inconsequential because the coupling end of the machine does not become unbalanced over time like the impeller does.

At the much higher frequencies of 23,391 rpm and 25,120 rpm for the original and revised rotors, respectively, the third mode is fundamentally different in nature from the first two modes. This is because it is the first free-free flexible rotor mode, meaning that it is unaffected by bearing stiffness at low stiffness values. In this case, the frequency is raised by the shaft modifications because of the reduced midspan mass. The high shaft strain energy of this mode introduces high modal stiffness and the high angular rotations introduce high modal mass due to rotary inertia. These make the bearing dynamic stiffness ineffective at low stiffness values, resulting in free-free rotor motion and high dynamic amplification factors. As the support stiffness is increased to around 500,000 lbf/in, this mode becomes susceptible to bearing stiffness and is raised in frequency like the other modes. Because of its high frequency relative to running speed, the third mode has minimal effect on the response in the operating range, making its effects inconsequential.

### *Damped Unbalance Response*

Computed rotor unbalance response at the bearings is shown in Figure 9 for the original and revised rotors. The unbalance was 4.5 oz-in applied at the impeller. As expected, the response rises to a significant peak at the first critical speed, and then falls off in the super resonant regime. Comparison of the two sets of curves reveals a beneficial 40 percent reduction in running-speed response at the impeller end from 0.41mils-pk to 0.22 mils-pk with the revised shaft. At the coupling end, the revised shaft reduces the response by 73 percent, from 0.28 mils-pk to 0.075 mils-pk. Since the bearing loads are roughly proportional to the bearing displacements, there is expected to be an accompanying reduction in dynamic bearing loading.

Because of the slight reduction in first-mode damping with the more flexible shaft, there is a moderate seven percent increase in impeller-end bearing response at the first critical speed. However, this is a minor increase compared to the much greater beneficial reduction in running speed response afforded by the flexible shaft. Careful selection of the final shaft diameter was required to insure that the damping at the first mode remained sufficient to control the unbalance response through the first critical speed. To compensate for the slight increase in critical speed response, a 20 percent reduction in the trip level vibration specification was recommended, thus protecting the machine against impeller rubs while traversing the first critical speed.

### *Response Amplification Factors*

The dynamic amplification factor for the first critical speed is given by

$$AF = \frac{N_{CR}}{N_2 - N_1} \tag{4}$$

where:

$N_{CR}$ = Rotor Speed at Maximum Amplitude (rpm)

$N_1, N_2$ = Rotor Speeds at 0.707 × Maximum Amplitude (rpm)

The computed first mode damped frequencies and amplification factors for the original and revised shafts are listed in Table 1. Reduction of the shaft stiffness raises the amplification factor from 1.04 to 2.13. Although the new value is higher, reflecting the decrease in damping, it is still well within the API recommended maximum value of approximately 8.0 for critical speeds that are well separated from the running speed. Consequently, the first critical speed would continue to be defined as well damped.

*Table 1. First Mode Response Summary.*

| Rotor-Bearing Configuration | Response Peak (rpm) | Amplification Factor |
|---|---|---|
| Original Rotor/Bearings | 4560 | 1.04 |
| Modified Rotor/Bearings | 3200 | 2.13 |

*Dynamic Bearing Loads*

The most important results of all are shown in Figure 10, where the computed dynamic bearing loads are plotted *vs* speed for the original and modified rotors. Inspection of these curves confirms the expected reduction in bearing dynamic loads at running speed when the shaft stiffness is reduced. With the original shaft, the impeller-end bearing experiences a very high dynamic load of 365 lbf at running speed. This is reduced beneficially by 48 percent to

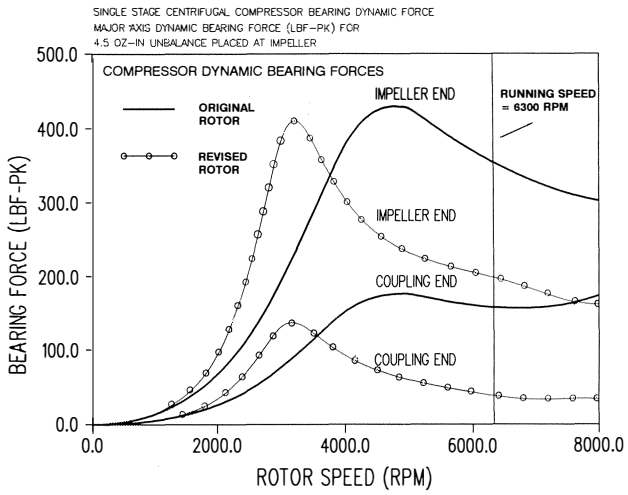


*Figure 10. Computed Compressor Bearing Dynamic Loads.*

190 lbf with the reduced-stiffness shaft. At the coupling end, the original 160 lbf dynamic load is reduced by 72 percent to 45 lbf.

Such a significant reduction in steady-state dynamic bearing loads is very beneficial to overall machine performance and reliability. Since bearing pad pivot wear is approximately a cubic function of the loads, the wear in the impeller end bearing is predicted to be reduced to

$$\frac{\text{New Wear Rate}}{\text{Orig. Wear Rate}} = \left[\frac{\text{New Load}}{\text{Old Load}}\right]^3 = \left[\frac{190}{365}\right]^3 = 0.14 \quad (5)$$

Thus, the reduction in shaft stiffness is predicted to lower the bearing wear rate to approximately 14 percent of the original value. Since the bearings were also upgraded from the original rocker-pivot tilting pad design, to the high load capacity spherical-pivot design, a dramatic improvement in overall bearing reliability was expected. This was confirmed by the improved performance history of the revised compressor, where the original three month service outages (for bearing overhauls) were extended to routine annual shutdowns for simple inspection and rebalancing.

*Measured Machine Response*

For verification of the analytical predictions, the actual machine unbalance response was recorded in both the original and modified compressors during a slow coastdown. The resulting rotor response near the bearings is illustrated in Figure 11 for both machines. Since the actual unbalance in both machines was not the same, it is not possible to compare the magnitudes in Figure 11 directly. Therefore, to develop a more reasonable comparison, a

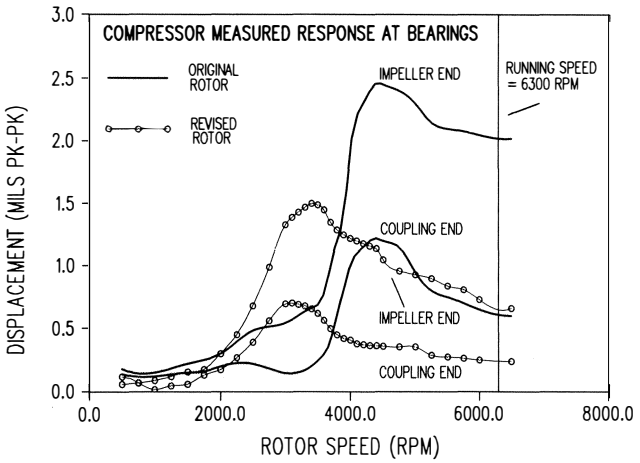


*Figure 11. Measured Compressor Unbalance Response at Bearings.*

second graph is plotted in Figure 12 representing the "adjusted" response of the revised rotor to better match the unbalance condition of the original rotor. This was done by increasing the revised rotor data by a factor that matches the data from both rotors at 1000 rpm (subresonant), where they are predicted analytically to be nearly equal under the same unbalance.

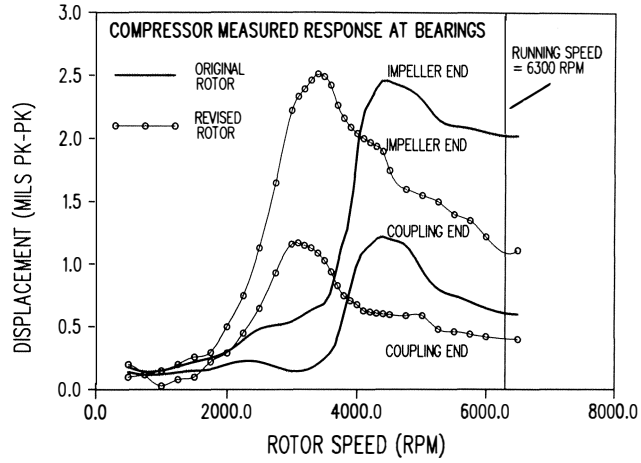


*Figure 12. Adjusted Compressor Unbalance Response at Bearings.*

Inspection of the data in Figures 11 and 12 confirms the predicted drop in the critical speed with the decrease in shaft stiffness. The measured critical speeds do not match exactly the analyses because of assumptions in the support model, bearing models, etc. However, the measured data does reveal very clearly the expected reduction in response at the running speed of 6300 rpm, where the revised rotor exhibits approximately 45 percent less unbalance response than the original rotor at the impeller end in the adjusted data. Since the bearing dynamic loads are approximately propor-

tional to the journal response amplitudes, the beneficial reduction in bearing loads is confirmed in the measured data.

*Stability Analysis*

A complete flexible rotor stability analysis was performed to assure continued rotordynamic stability in the more flexible rotor. This involves computation of the damped natural frequencies and corresponding logarithmic decrements at the rotor operating speed for a range of bearing dimensions that are varied parametrically until maximum logarithmic decrements are achieved. The stability rotor model is the same as the response model, with speed-dependent bearing coefficients, gyroscopics, and rotary inertia effects.

Crosscoupling effects from all sources including the impeller, seals, and bearings, combine with the available damping to determine the net machine stability. Alford [5] developed a procedure for estimating the aerodynamic crosscoupling in a compressible-flow machine as a function of the stage torque and blade geometry. Using his approach, the aerodynamic crosscoupling may be estimated (very approximately) as

$$K_{xy} = -K_{yx} = \frac{\beta T}{2Rh} \quad (6)$$

where:

T = Torque (lbf-in)
R = Blade mean radius (in)
h = Blade axial length at tip (in)
β = Cross-coupling factor (21 for single-stage compressor)

For the 3500 hp compressor running at 6300 rpm, the cross-coupling becomes

$$K_{xy} = -K_{yx} = 21(35{,}000\text{lbf-in})/2(13\text{in})(3\text{in})$$
$$= 9{,}400 \text{ lbf/in}$$

Rotor stability is computed at the maximum running speed (6300 rpm). The computed logarithmic decrements must be positive for stable operation, and should generally be above 0.2 for flexible rotors. The computed logarithmic decrements for the first two real forward modes are listed in Table 2 for the original and revised rotor configurations. The first mode stability is lowered slightly with the new configuration, while the second mode stability is raised. All of the values are well above the recommended minimum of 0.2, thus assuring continued stability with the modified rotor.

*Table 2. Stability and Damped Frequency Summary.*

| Rotor-Bearing Configuration | Mode | Damped Frequency (rpm) | Logarithmic Decrement |
|---|---|---|---|
| Original Rotor/Bearings | 1st Forward | 4560 | 2.33 |
| | 2nd Forward | 9600 | 0.74 |
| Modified Rotor/Bearings | 1st Forward | 3200 | 1.34 |
| | 2nd Forward | 7350 | 1.08 |

*Torsional Frequency Analysis*

A torsional natural frequency analysis of the complete rotor train was conducted to assure that the reduced diameter shaft does not shift a fundamental frequency too close to a harmonic of running speed. Possible sources of torsional excitation include motor pole passing frequencies at integer multiples of motor speed, and gear ellipticity excitations at integer multiples of each gear. For this rotor train with low and high speeds of 1800 rpm and 6300 rpm, the torsional frequencies that must be avoided are listed in Table 3.

The first four torsional frequencies and mode descriptions for the original and optimized rotor systems are listed in Table 4. All of the frequencies, both before and after the shaft modifications,

*Table 3. Potential Torsional Excitation Frequencies.*

| Low Speed Side Frequencies (cpm) | High Speed Side Frequencies (cpm) |
|---|---|
| 1 × 1800 = 1800 | 1 × 6300 = 6300 |
| 2 × 1800 = 3600 | 2 × 6300 = 12600 |
| 3 × 1800 = 5400 | 3 × 6300 = 18900 |

are at least 10 percent removed from the nearest potential excitation frequency, thus assuring that the new rotor system will be free from adverse torsional resonances.

*Table 4. Torsional Natural Frequency Summary.*

| Mode Description | Original Train Frequency (cpm) | Modified Train Frequency (cpm) |
|---|---|---|
| Armature *vs* Impeller | 1546 | 1400 |
| Gears+Coupling *vs* Armature+Impeller | 4606 | 3240 |
| Armature Second Mode | 10030 | 10029 |
| Armature *vs* Coupling | 17790 | 17784 |

*Torsional Stress Analysis*

Torsional stresses associated with steady-state and transient operating torques were examined to assure that the new rotor could safely carry the machine operating torques. The maximum torsional shear stress of a solid shaft is

$$\sigma_{max} = \frac{2T}{\pi R^3} \quad (7)$$

where:

$\sigma_{max}$ = Maximum tensile stress (lbf/in2)
T = Shaft torque (lbf-in)
R = Shaft radius (in)

*Steady State Torsional Stresses*

The steady state running speed torque for the high speed side carrying 3500 HP at 6300 rpm is:

$$T = \frac{(3500)(63{,}000)}{6300}$$
$$= 35{,}000 \text{ lbf-in}$$

The corresponding maximum steady state torsional stress for the revised shaft occurs at the minimum diameter of 2.8 in. Thus, from Equation (7), the stress becomes:

$$\sigma_{max\ static} = \frac{2(35{,}000 lbf\text{-}in)}{\pi(1.4in)^3}$$

$$= 8120\ lbf\text{-}in^2$$

Since the safe operating limits for steady stresses in high-grade steel are considered to be above 30,000 psi, this value is very acceptable.

*Transient Torsional Stresses*

During startup, the rotor is subjected to a high transient angular acceleration which adds to the steady state torque to give a peak transient torque-induced stress. The transient acceleration torque for this machine is:

$$T_{acc} = I\alpha$$

$$= \frac{25{,}000\ lbm\text{-}in^2}{386\ \frac{lbm\text{-}in}{lbf\text{-}s^2}} \times \frac{6300rpm}{6sec} \times \frac{2\pi rad}{rev} \times \frac{1\ min}{60sec}$$

$$= 7120\ lbf/in$$

The corresponding stress is given by Equation (7) as:

$$\sigma_{max\ acc} = \frac{2(7120 lbf\text{-}in)}{\pi(1.4in)^3}$$

$$= 1650\ lbf/in^2$$

The maximum peak transient torsional stress is the combined static and acceleration stress:

$$\sigma_{max\ transient} = \sigma_{max\ static} = \sigma_{max\ acc}$$

$$= 8120\ lbf/in^2 + 1650\ lbf/in^2$$

$$= 9770\ lbf/in^2$$

The maximum transient stress of 9,770 psi is acceptable since the allowable operating cyclic stress for high grade steel is well above 10,000 psi.

*Shaft Bending Stresses*

To assure that the modified rotor will not experience excessive bending stresses from the shaft moments caused by unbalance, the unbalance computations were repeated to plot the moments induced.

The computed shaft moments *vs* speed at all five reduced-diameter stations are plotted in Figure 13 for the same conservative unbalance of 4.5 oz-in placed at the impeller. The maximum shaft moment occurs at station 5, with a magnitude of approximately 6000 lbf-in at the critical speed. The corresponding maximum stress is given by:

$$\sigma_{shaft\ bending} = \frac{MC}{I} \qquad (8)$$

where:

M = Shaft Moment (lbf-in)
C = Outer Surface Radius (in)
I = Section Moment of Inertia ($in^4$)
= 3.02 $in^4$

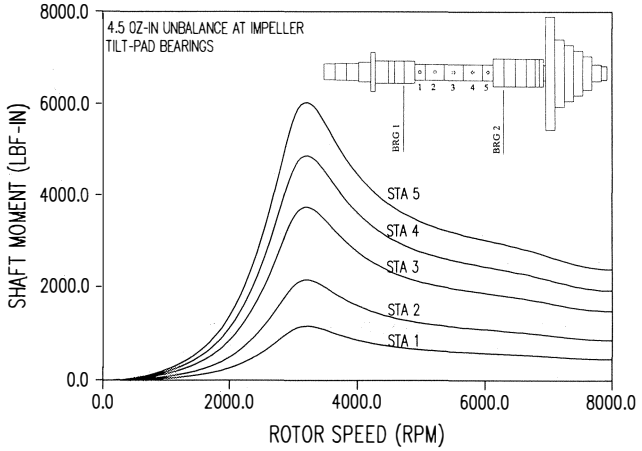


*Figure 13. Computed Compressor Maximum Shaft Moments* Vs *Speed.*

Thus, the maximum bending stress at the critical speed becomes:

$$\sigma_{max\ bending} = \frac{(6000\ lbf\text{-}in)\ (1.4\ in)}{3.02\ in^4}$$

$$= 2780\ lbf/in^2$$

Again, this is completely insignificant compared to the stress capability of the shaft material, making the revised shaft free from excessive bending stresses.

*Bearing Upgrades*

Many authors [6, 7, 8, 9] have analyzed tilting pad bearings and compared the features of various types of pad pivots. Illustrated in Figure 14 are cross sections of the original rocker-pivot tilting pad bearings and the replacement spherical-pivot tilting pad bearings. The rocker-pivot pads can tilt freely in the axial direction, but have almost no tilt capability in the tangential direction, because of the line contact pivots. This reduces their capability to accommodate shaft misalignment and can lead to high edge loading. Also, the line contact pivot is more susceptible to wear and fretting due to the high contact stresses.

The spherical contact pivot offers the advantage of full tilt capability in all directions, making it fully self-aligning, even for severe shaft misalignment. The spherical pivot design also provides superior load distribution, reducing the contact stresses and improving the pivot load capability. This is illustrated in Figure 15, where the pivot contact stresses *vs* radial unit load are plotted for

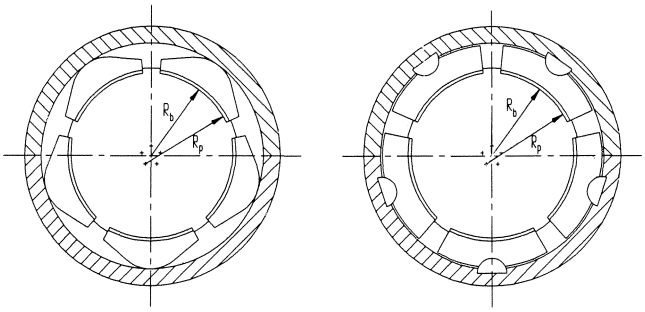


*Figure 14. Original Rocker Pivot and Replacement Spherical Pivot Tilting Pad Bearings.*

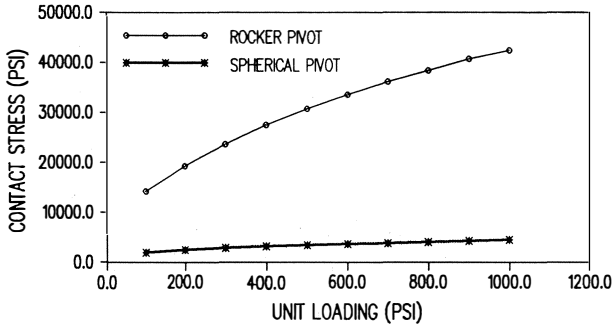


*Figure 15. Contact Stresses in Rocker Pivot and Spherical Pivot Bearings.*

both the rocker pivot and the spherical pivot, indicating as much as 10 times higher stress in the rocker pivot [6].

The design parameters and stiffness and damping coefficients are listed in Table 5 for the optimized tilting pad bearings at 6300 rpm. The bearings are installed in the load-between-pad orientation, yielding nearly symmetric (equal) stiffness and damping properties. The low cross coupled stiffness coefficients are responsible for the high rotordynamic stability discussed earlier. Oil flow requirements correspond to a 30°F temperature rise at the computed power loss.

## CONCLUSION

The potential for reducing running-speed bearing loads through the reduction of shaft stiffness have been illustrated through a case study in which a 48 percent decrease in computed bearing loads was achieved, yielding a dramatic improvement in machine reliability. The primary conclusions which may be drawn from the discussion presented are as follows:

- Reduction of shaft stiffness in certain types of turbomachines can potentially lower the dynamic bearing loads at running speed without adversely affecting the rotor integrity or the rotordynamic characteristics of the machine.

- The reduction of bearing dynamic loads, in combination with the installation of high capacity spherical pivot tilting pad bearings, can dramatically improve the operating reliability of machines such as the single stage overhung compressor discussed.

- As in any major design modification, caution must be exercised in the design and analysis stages to avoid subjecting a machine to instabilities, excessive unbalance response, or high shaft stresses.

## APPENDIX

### *Single-Mass Rotor Equations of Motion*

The principle of super-resonant response can be illustrated by deriving the equations of motion for the simple single mass rotor shown in Figure A-1. Commonly known as the Jeffcott rotor, the symmetric single-mass rotor may be easily modeled mathematically without consideration of gyroscopic or rotary inertia effects. Therefore, the Jeffcott rotor may be treated as a single degree of freedom rotor having only one critical speed in the operating range.

The animated first critical speed of the Jeffcott rotor is illustrated in Figure A-2. The bearing stiffnesses were adjusted to represent the approximate dynamic stiffness of a simple 3/8 in diameter two-axial-groove oil lubricated bearing at 2500 rpm. Because the disk is positioned symmetrically between similar bearings, the disk motion is purely translational.

*Table 5. Spherical-Pivot Bearing Geometry and Dynamic Characteristics at 6300 RPM.*

| | Coupling End | Impeller End |
|---|---|---|
| Bearing Type | 5 Pad Tilting Pad Load Between Pad Spherical Pivot | 5 Pad Tilting Pad Load Between Pad Spherical Pivot |
| Nominal Shaft Dia. (in) | 4.0005 | 4.9984 |
| Pad Axial Length (in) | 2.80 | 3.50 |
| L/D Ratio | 0.7 | 0.7 |
| Pad Arc Length (deg) | 68.0 | 68.0 |
| Static Load (lbf) | -144.9 | 721.7 |
| Nominal Diametral Clearances (mils): | | |
| Bearing Set Clearance | 8.0 | 7.0 |
| Pad Clearance | 8.0 | 10.0 |
| Preload | 0.0 | 0.3 |
| Oil Type | 150 SUS @ 100 F | 150 SUS @ 100 F |
| Inlet Temperature (F) | 110 | 110 |
| Inlet Pressure (psi) | 20 | 20 |
| Reqd. Flowrate (gpm) | 2.5 | 6.2 |
| Power Loss (hp) | 3.12 | 8.55 |
| Ecc. Ratio (dim) | 0.16 | 0.19 |
| Kxx (lbf/in) | 222,000. | 591,000. |
| Kxy (lbf/in) | -21,000. | -10,200. |
| Kyx (lbf/in) | 20,900 | 15,900. |
| Kyy (lbf/in) | 230,000. | 694,000. |
| Cxx (lbf-sec/in) | 1030. | 2370. |
| Cxy (lbf-sec/in) | 34. | 28. |
| Cyx (lbf-sec/in) | -34. | -15. |
| Cyy (lbf-sec/in) | 1043. | 2544. |

In the absence of angular (rotational) motion in the mode shape, there are no gyroscopic or rotary inertia effects, making the problem similar to a single degree of freedom spring-mass-damper model [10]. For such a system, the differential equation of motion is

$$M\ddot{X} + C\dot{X} = KX = Mu_b\omega^2 e^{i\omega t} \qquad \text{(A-1)}$$

where:

X = Disk radial displacement (in)
M = Rotor modal mass (lbm)

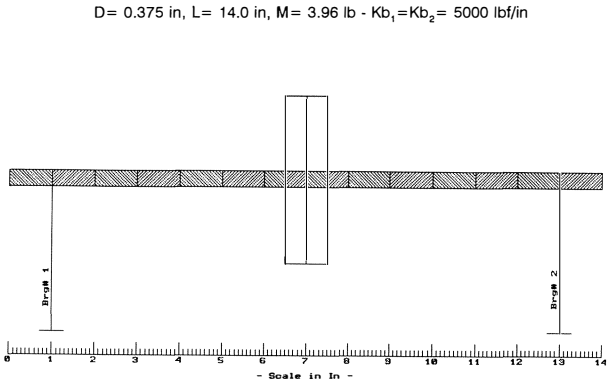


*Figure A-1. Single-Mass Jeffcott Rotor Model.*

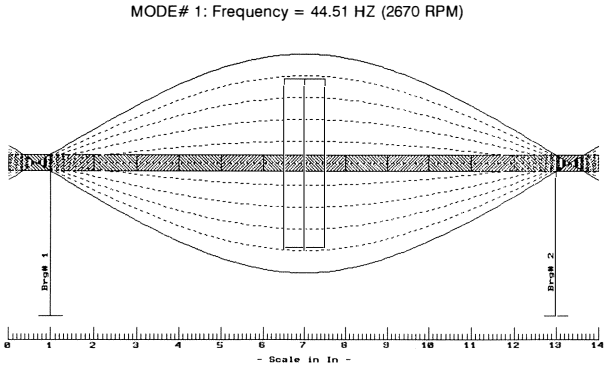


*Figure A-2. Jeffcott Rotor First Undamped Mode Shape.*

C = Rotor modal damping (lbf-s/in)
K = Rotor modal stiffness (lbf/in)
$u_b$ = Unbalance eccentricity (in)
$\omega$ = Rotor speed (rad/sec)

The displacement may be expressed in complex notation as:

$$X(t) = X_o e^{i\omega t} \tag{A-2}$$

The derivatives then become:

$$\begin{aligned} \dot{X}(t) &= i\omega X_o e^{i\omega t} \\ \ddot{X}(t) &= -\omega^2 X_o e^{i\omega t} \end{aligned} \tag{A-3}$$

Substituting these into the equation of motion gives:

$$X_o e^{i\omega t}(-\omega^2 M + i\omega c + K) = M u_b \omega^2 e^{i\omega t} \tag{A-4}$$

Dropping the time dependence and rearranging gives the unbalance response magnitude as:

$$\begin{aligned} X_o &= \frac{M u_b \omega^2}{K - \omega^2 M + i\omega C} \\ &= \frac{u_b}{\frac{K}{\omega^2 M} - 1 + i\frac{C}{\omega M}} \end{aligned} \tag{A-5}$$

For further simplification, the dimensionless frequency and damping ratios are defined as:

$$\begin{aligned} r &= \frac{\omega}{\omega_n} = \frac{\omega}{\sqrt{K/M}} \\ \xi &= \frac{C}{C_c} = \frac{C}{2\sqrt{K/M}} \end{aligned} \tag{A-6}$$

Substituting these into the response equation gives:

$$X_o = \frac{u_b}{\frac{1}{r^2} - 1 + i\frac{2\xi}{r}} \tag{A-7}$$

Multiplying the numberator and denominator by $r^2$ gives:

$$X_o = u_b \left[\frac{r^2}{1 - r^2 + i2\xi r}\right] \tag{A-8}$$

Solving for the real magnitude of the complex denominator gives the final response magnitude in terms of the unbalance eccentricity:

$$X_o = u_b \left[\frac{r^2}{\sqrt{(1 - r^2)^2 + (2\xi r)^2}}\right] \tag{A-9}$$

*Single-Mass Rotor Response Characteristics*

Having developed the general response expression of Equation (A-9), the particular response characteristics in the subresonant, resonant, and super resonant regimes may be computed using the following three values of the frequency ratio:

$$\begin{aligned} r = \frac{\omega}{\omega_n} &\simeq 0 \text{ (subresonant)} \\ &= 1 \text{ (resonant)} \\ &\simeq \infty \text{ (super resonant)} \end{aligned}$$

*Subresonant Response*

Well below the critical speed, the frequency ratio becomes very small, approaching zero in the limit as the rotor approaches slow roll. Substituting r = 0 into the response expression of Equation (A-9) gives the limiting subresonant response as:

$$\begin{aligned} X_{o_{\text{sub-resonant}}} &\simeq u_b \left[\frac{0}{\sqrt{1 + 0}}\right] \\ &\simeq 0 \end{aligned} \tag{A-10}$$

Therefore, the response is predicted to approach zero at speeds well below the critical speed.

*Resonant Response*

At the critical speed, the frequency ratio is nearly 1, giving the critical speed response from Equation (A-9) as:

$$\begin{aligned} X_{o_{\text{resonant}}} &= u_b \left[\frac{1}{\sqrt{(0)^2 + (2\xi)^2}}\right] \\ &= u_b \left[\frac{1}{2\xi}\right] \\ &= \frac{u_b}{2\xi} \end{aligned} \tag{A-11}$$

As expected, the predicted critical speed response depends only on the unbalance eccentricity and the damping ratio. Decreasing the damping raises the response exponentially to infinity at zero damping, while increasing the damping lowers the response to a limiting value of zero at infinite damping.

*Super Resonant Response*

At speeds well above the first critical speed, the value of r becomes large. The limiting value of response will then correspond to a frequency ratio of $r = \infty$, giving the limiting response from Equation (A-9) as:

$$X_{o_{\text{super resonant}}} \simeq u_b \left[ \frac{\infty^2}{\sqrt{(1-\infty^2)^2 + (2\xi\infty)^2}} \right] \simeq u_b \left[ \frac{\infty^2}{\sqrt{\infty^4}} \right] \simeq u_b \quad \text{(A-12)}$$

Therefore, the synchronous response at speeds well above the first critical speed is predicted to approach the static unbalance eccentricity, $u_b$.

The computed unbalance response *vs* speed is illustrated in Figure A-3 for the Jeffcott rotor with unbalance placed at the disk. Bearing coefficients corresponding to a simple 3/8 in diameter two-axial-groove oil lubricated bearing were used. The unbalance used was 0.035 oz-in, giving a mass eccentricity for the 3.55 lb rotor disk of:

$$U_b = \frac{0.035 \text{ oz-in}}{(3.55\text{lbm})(16\text{oz/lbm})} = 0.00061 \text{ in} \quad \text{(A-13)}$$

Examination of Figure A-3 confirms the response predictions of Equation (A-9), giving subcritical response of nearly zero at very low speed, and super critical response that asymptotically approaches the unbalance eccentricity of 0.61 mils given in Equation (A-13).

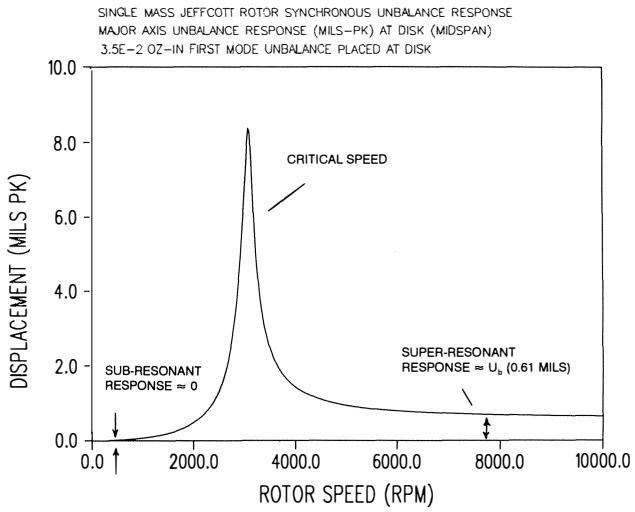


*Figure A-3. Jeffcott Rotor Unbalance Response.*

## REFERENCES

1. Kirk, R. G. and Gunter, E. J., "The Effects of Support Flexibility and Damping on the Synchronous Response of a Single Mass Flexible Rotor," Journal of Engineering for Industry, ASME Trans., 94.1 Series B, pp. 221-232 (February 1972).
2. Salamone, D. J. and Gunter, E. J., "Synchronous Unbalance Response of an Overhung Rotor with Disk Skew," ASME Journal of Engineering for Power, *102*, pp. 749-755 (October 1980).
3. Nicholas, J. C., "Improving Critical Speed Calculations Using Flexible Support Modal Analysis Compliance Data," *Proceedings of the Fifteenth Turbomachinery Symposium*, The Turbomachinery Laboratory, The Texas A&M University System, College Station, Texas, pp. 69-78 (1986).
4. Gunter, E. J., Hobbs, A., and Phelps, E., "Dynamic Characteristics of an Overhung P/A Fan in Rolling Element and Fluid Film Bearings," *Proceedings of the Third International Symposium on Transport Phenomena and Symposium of Rotating Machinery*. (1990).
5. Alford, J. S., "Protecting Turbomachinery from Self-Excited Rotor Whirl," Journal of Engineering for Power, pp. 333-344 (October 1965).
6. Zeidan, F. Y., "Fluid Film Bearing Fundamentals and Failure Analysis," *Proceedings of the Twentieth Turbomachinery Symposium*, The Turbomachinery Laboratory, The Texas A&M University System, College Station, Texas, pp. 161-186 (1991).
7. Allaire, P. E. and Flack, R. D., "Design of Journal Bearings for Rotating Machinery," *Proceedings of the Tenth Turbomachinery Symposium*, The Turbomachinery Laboratory, The Texas A&M University System, College Station, Texas, pp. 25-45 (1981).
8. Nicholas, J. C., "Fundamental Bearing Design Concepts for Fixed Lobe and Tilting Pad Bearings," Dresser-Rand Technical Publications, pp. 51-78 (1987).
9. Armentrout, R. W. and Paquette, D. J., "Rotordynamic Characteristics of Flexure-Pivot Tilt-Pad Journal Bearings," ASME/STLE Tribology Conference, Philadelphia, Pennsylvania (1992).
10. Vance, J. M., *Rotordynamics of Turbomachinery*, New York, New York: John Wiley & Sons (1988).

## ACKNOWLEDGEMENTS

Development of the compressor upgrades and modifications was conducted by CentriMarc division of IMO Industries in cooperation with the Chino Mines Company of Hurley, New Mexico. The authors wish to thank CentriMarc and the Chino Mines Company for their involvement.